



Plumes anchored by a high viscosity lower mantle in a 3D mantle convection model featuring dynamically evolving plates

J. P. Lowman,^{1,2} A. D. Gait,³ C. W. Gable,⁴ and H. Kukreja¹

Received 14 July 2008; revised 28 August 2008; accepted 12 September 2008; published 14 October 2008.

[1] Previous studies have shown that 3D vigorously convecting systems featuring plate-like surface motion and lower mantle viscosities much greater than the upper mantle viscosity can yield long lived intraplate plumes if plate boundaries remain fixed. We investigate whether plumes originating in a lower mantle 90 times more viscous than the upper mantle will maintain relatively fixed positions when dynamic plate evolution is present. We compare the findings from a pair of calculations featuring four plates in a $3 \times 3 \times 1$ periodic Cartesian geometry model. In both calculations, plate velocities are determined dynamically in response to the stresses acting on the viscously defined lithosphere. In one case plate boundaries are held fixed, in the second dynamically determined plate evolution is enabled. In both cases, long lived mantle plumes are observed. Moreover, the locations of the plumes remain relatively fixed even as plates systematically evolve to a completely different arrangement from their initial configuration. **Citation:** Lowman, J. P., A. D. Gait, C. W. Gable, and H. Kukreja (2008), Plumes anchored by a high viscosity lower mantle in a 3D mantle convection model featuring dynamically evolving plates, *Geophys. Res. Lett.*, *35*, L19309, doi:10.1029/2008GL035342.

1. Introduction

[2] Hotspot tracks associated with mantle plumes imply the latter must be stationary or moving independently of the motion of the over-riding plate. Moreover, plume positions (or trajectories) can apparently remain unaffected by plate evolution for extensive periods. A variety of models and studies have been put forth with the common objective of providing an explanation for hotspot fixity and longevity [Jellinek and Manga, 2004]. This study focuses on the effect of mantle viscosity stratification on plume motion in a convection model featuring evolving plates.

[3] Early mantle convection models demonstrated that stationary mantle plumes could not be obtained in two-dimensional systems featuring plates moving with comparable velocities to the vertical motion in the plumes [Lux *et al.*, 1979]. However, later 3D models that feature dynamically consistent time-dependent plate velocities determined by buoyancy field evolution, show that three-dimensional

plumes can occupy relatively fixed locations for periods in excess of a mantle transit time [e.g., Zhong *et al.*, 2000; Lowman *et al.*, 2004; Quéré and Forte, 2006]. A key feature of the later studies includes a significant increase in lower mantle viscosity (by a factor of 30–90) relative to the viscosity of the upper mantle. The impact of the stratification of the mantle's viscosity on plume motion and its ability to lengthen plume lifetimes and stabilize positions has been rigorously demonstrated using geodynamic models [e.g., Steinberger and O'Connell, 1998].

[4] Previous studies [Zhong *et al.*, 2000; Davies, 2005; Quéré and Forte, 2006] have concluded that downwelling locations control the locations of upwellings, which tend to form at stagnation points on the lower boundary of a vigorously convecting system. This raises the question of whether the fixed plumes observed in the earlier studies persist when plate boundary locations and plate sizes undergo substantial evolution. Here, we compare plume motion in two calculations. In both cases plate velocity is dynamically determined by a force balance method [Gable *et al.*, 1991]. In the first, plate boundaries remain fixed during the calculation. In the second, plate boundaries migrate, leading to systematically and continually changing plate shape and size.

2. Model Description

[5] The systems modeled feature rheologically defined finite thickness plates incorporated in a Cartesian geometry mantle convection model. We solve for infinite Prandtl number convection in an incompressible Boussinesq fluid with a Newtonian rheology [e.g., Gait *et al.*, 2008]. The calculations use 324 Fourier modes in each of the horizontal directions and 129 nodes in the vertical direction to obtain solutions with periodic side walls in $3 \times 3 \times 1$ solution domains. The upper and lower boundaries are isothermal and the base is free-slip. All parameters appearing in the Bénard-Rayleigh number, Ra_B , [e.g., Gait *et al.*, 2008] are spatially constant, with the exception of the viscosity, which is depth-dependent. The viscosity in the models examined has a nondimensional value of 1.0 in the region extending from the base of the model plates to a depth of $0.231d$, where d is the depth of the combined plate-mantle system. Viscosity in the lower mantle increases from 1 to 90 (at the base of the solution domain) following the logarithmic increase described by Gait *et al.* [2008]. Based on the viscosity at the base of the plates, $Ra_B = 5 \times 10^7$. The models are heated from within, as well as from below. The nondimensional heating rate, H , is 15.

[6] The stiffness of the Earth's cold lithosphere is modeled by specifying plates that are 1000 times more viscous than the mantle immediately below. The plate thickness is

¹Department of Physical and Environmental Sciences, University of Toronto Scarborough, Toronto, Ontario, Canada.

²Also at Department of Physics, University of Toronto, Toronto, Ontario, Canada.

³School of Mathematics, University of Manchester, Manchester, UK.

⁴Hydrology, Geochemistry and Geology Group, Earth and Environmental Sciences Division, Los Alamos National Laboratory, Los Alamos, New Mexico, USA.

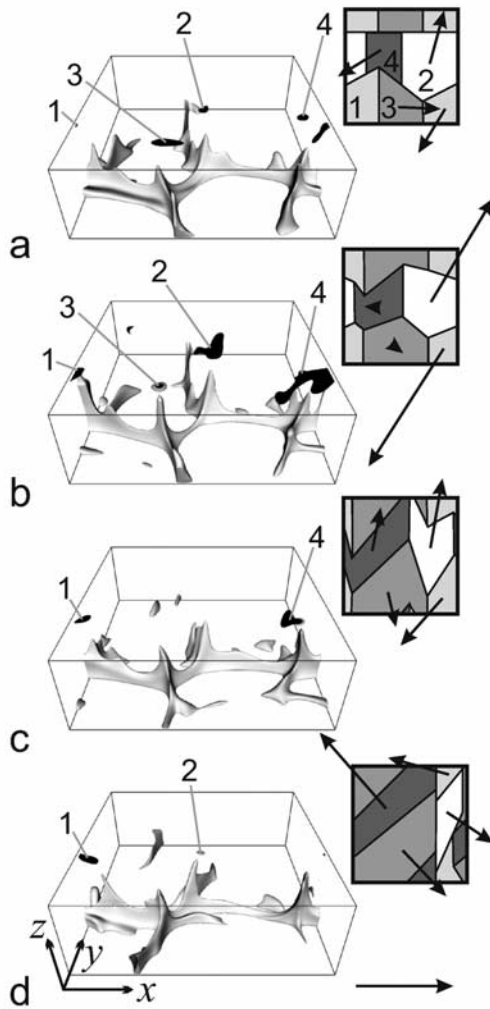


Figure 1. (a–d) Isosurfaces of temperature relative to the mean temperature at the same depth (the residual-temperature) and the locations of the hot anomalies discussed in the text. The isosurface value is 0.14. Also shown are maps of the surface indicating the locations and shapes of the four distinct evolving plates (labelled in Figure 1a). The arrows on the maps indicate the direction and magnitude of plate motion. The arrow drawn at the bottom right of the figure has a length that is linearly proportional to the arrows on the maps and a nondimensional velocity of 2000 (i.e., a particle moving at this velocity would travel a distance equal to the depth of the mantle 2000 times per diffusion time). This translates to 1.714 mean surface transit velocities.

fixed at $0.047d$. The models examined feature four idealized polygonal plates (see Figure 1a) in an initial configuration characterized by eight triple junctions. Plate boundaries are formed by connecting the triple junctions and the evolution of plate size and shape is determined by migrating the model triple junctions with the mean velocities of the three associated plates. Although highly simplified in comparison to the motion of real triple junctions, our modelling method [Gait *et al.*, 2008] does allow the evolution of the triple junctions (and therefore the plate dimensions) to dynami-

cally respond to changes in the magnitudes of the plate velocities.

[7] The time-dependent plate velocities are calculated using a force balance method [e.g., Gable *et al.*, 1991; Monnereau and Quéré, 2001] to ensure that the motion of the plates remains in dynamic equilibrium with the buoyancy forces in the thermally evolving lithosphere and mantle. At all times, this method satisfies the condition that the net shear stress on the base of the lithosphere resulting from purely plate driven flow is balanced by the net shear stress resulting from buoyancy-driven flow. This method for calculating plate velocities has been described in detail elsewhere [e.g., Gable *et al.*, 1991] and found to give excellent agreement with completely independent plate modelling methods [e.g., King *et al.*, 1992; Koglin *et al.*, 2005].

[8] The initial temperature field for our models is obtained by integrating forward a calculation with the fixed plate geometry specified in our Model A (see Figure 1a). Once the system has reached a statistically steady state, a snapshot of the temperature field is taken at a random time to provide the initial condition for the calculations described. Model B differs from Model A by allowing for the evolution of plate size and shape, as described above.

3. Results

[9] Figure 1a depicts an isosurface in the residual-temperature field [e.g., Tackley, 1996; Zhong *et al.*, 2000] calculated from the initial thermal field specified in Models A and B. The temperature field associated with the plates has been removed in order to view anomalies in the mantle below. Figures 1b–1d show three later snapshots from Model B of the same 0.14 residual-temperature isosurface. The temporal separation of the snapshots is 0.0012 diffusion times or 1.4 surface transit times ($=1.4d/(\text{the temporally averaged mean surface velocity from Model B})$). Temperature fields and time series of the plate velocity direction and magnitude from the two models were presented previously by Gait *et al.* [2008]. Although the magnitudes of the plate velocities in Model A fluctuate by a factor of 3 during the period we examine, the convective planform changes very little from that shown in Figure 1a. In contrast, movement of the plate boundaries in Model B results in a significant change in the location of downwellings during an equivalent period. The isosurfaces reveal a linear network of anomalously hot features in the lower mantle punctuated by the appearance of columnar anomalies that extend towards the surface. Four distinct hot anomalies are identified at a depth of $0.05d$ by a horizontal slice that shades in black all residual temperatures in excess of 0.14. Each is associated with an underlying hot columnar anomaly in the lower mantle and corresponds to the head of a thermal plume connected to the lower thermal boundary layer of the system.

[10] During the time period depicted, the surface area and shape of the plates in Model B change significantly. The motion of the plate boundaries is strongly reflected by changes in the positions of the cold thermal features [Gait *et al.*, 2008]. However, the positions of the hot lower mantle anomalies remain relatively stable and fixed.

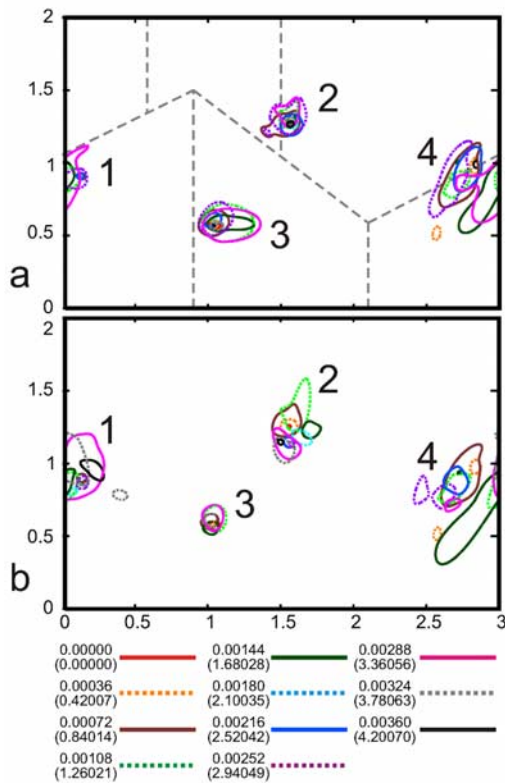


Figure 2. Residual-temperature contours for a value of 0.14 at a depth of $0.063d$ in Models (a) A and (b) B. Different colors correspond to the nondimensional times indicated at the bottom of the figure. Surface transit times are given in parentheses. Time 0.00000 marks the start of the calculation. The axes indicate distance in units of d using the co-ordinate system shown in Figure 1.

[11] In order to identify the locations of hot anomalies, in Figure 2 we plot the 0.14 residual-temperature contours at a depth of $0.063d$ from Model A (Figure 2a) and Model B (Figure 2b). All of the hot anomalies revealed by these contours occur in the region of the solution domain corresponding to $y < 2$ (see the co-ordinate system indicated in Figure 1) thus each plot ignores one-third of the surface.

[12] In both models, the anomalies form four distinct clusters that are labeled with the numeric tags used to identify the hot plume heads indicated in Figure 1a. In addition to the residual-temperature contours, Figure 2a also shows the location of the fixed plate boundaries specified in that model (dashed lines). Figure 2a shows that the hot anomalies 1, 2 and 3 sit below the plates numbered correspondingly in Figure 1a. The fourth anomaly lies roughly in the region coinciding with a plate boundary (between plates 1 and 2) at time 0.0.

[13] Figure 2a shows that the hot anomalies associated with the plumes in Model A endure throughout the period examined. In particular, anomalies 2 and 3 are marked by contours associated with the initial and final times (red and black). Anomalies 1 and 4 fluctuate more in intensity but also exist throughout the time period examined. In addition to their longevity, the plume associated anomalies are characterized by their fixity, although the size and shape of the anomalies changes in response to pulses in the heat

carried by the underlying plume and variations in the velocity of the overlying plate.

[14] Figure 2b shows that despite the evolution of the plates boundaries in Model B, the four hot anomalies stay relatively close to their initial positions, as in Model A. This is despite the fact that the evolution of the surface results in different plates moving over the anomalies, causing significant variations in the surface velocities and upper mantle flow. Similarly, the location of the downwelling sheets in the model shift and migrate substantially but, during the period examined, have little effect on the upwellings anchored in the lower mantle.

[15] Figure 3 depicts an overhead view of an area with nine times the surface dimensions of our models. The red square at the center shows the boundaries of the solution domain of Model A and the line segments within the square show the positions of the fixed plate boundaries. Within the red box we use square markers to show the locations of the hottest points in anomalies 1-4 from Model A. The color of the markers corresponds to the color/time convention introduced in Figure 2 and therefore indicates position as a function of time. The markers are rendered in chronological order so that markers corresponding to more recent times are placed over those from earlier times in cases where the hotspot position has not moved. For anomalies 1-3, the final positions (at diffusion time 0.00360; surface

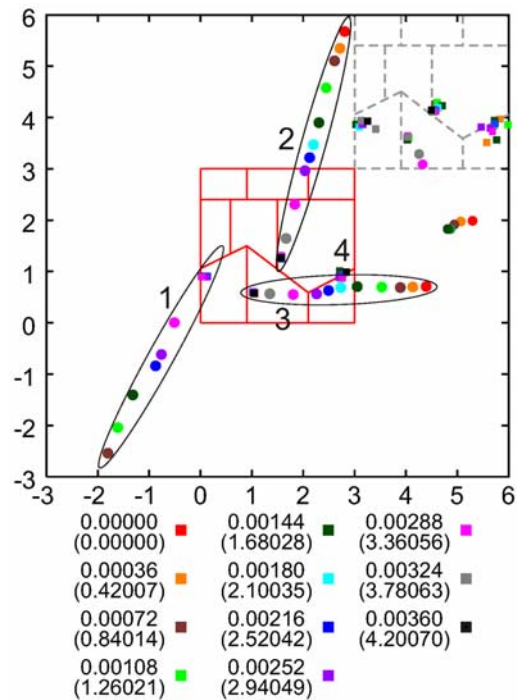


Figure 3. Locations of the hottest points (hotspots with a minimum residual temperature of 0.14) associated with anomalies 1-4 (squares). The anomalies from Model A are shown within the central map (outlined in red). Anomalies from Model B are shown within the bounds of the map at the upper right (grey dashed outline). The circular markers represent hotspot tracks formed by the corresponding anomaly (see the text for further detail). The clusters of circular markers near co-ordinates (4.25, 3.25) and (5, 2) are associated with anomaly 3 in Model B at (4, 3.5).

transit time 4.2) of particles released from the locations marked by the squares is indicated with a circular marker of corresponding color. Each circular marker has been advected with the velocity of the over-riding associated plate since its release at the time corresponding to its color. The circular markers form chains akin to hotspot tracks with lengths that indicate the velocity of the plates relative to any motion of the associated hot anomaly. We do not plot a track corresponding to anomaly 4 because it is not confined within the interior of a single plate.

[16] At the upper right corner of Figure 3 we show a second map of the initial plate boundary configuration (in a location consistent with the periodic boundaries specified in the calculations and the position of the first map). The area confined within the second map is used to represent the surface of Model B. The square markers within this region of Figure 3 show the locations of the hottest points from anomalies 1–4 in Model B. Due to the evolution of the plate boundaries, hot anomalies 1, 2 and 4 are each passed over by more than one plate. Consequently, their associated tracks are incoherent because at different times the associated markers are carried by different plates. However, anomaly 3 remains below plate 3 for the entire period examined and we can calculate and plot a hotspot track in this case following the approach used for the Model A data. In Model B, plate 3 sharply changes direction between diffusion times 0.0011 and 0.0013 (surface transit times 1.28 and 1.52) from a path angled at approximately 45° to the positive x -axis to a direction pointing roughly -70° from the positive x -axis. (This change in motion carries the marker chain of circles formed between times 0.00000 and 0.00144 (i.e., during the first 1.68 surface transit times) on a -70° bearing from anomaly 3.) During the change in direction, the magnitude of the plate velocity drops to almost zero before rising to a velocity greater than the initial plate velocity. Following the change in direction there is a drop in the intensity of anomaly 3 and the hot spot does not exceed the 0.14 residual-temperature threshold value we use to identify the hot anomalies until we sample the temperature field at time 0.00288 (3.36 transit times). A similar decrease in the intensity of the anomaly in Model A is not observed and indicates that the upwellings in Model B, although very stationary, are affected by the time-dependence of the system.

4. Discussion and Conclusions

[17] Our choice of Rayleigh number and internal heating rate in Models A and B assumes a mean thermal diffusivity for the mantle of order $10^{-6} \text{ m}^2 \text{ s}^{-1}$ and a superadiabatic temperature difference of approximately 3000°C across the mantle. The nondimensional heating rate ($H = 15$) is based on the assumption that the rate of internal heating in the mantle is $4.7 \times 10^{-12} \text{ W kg}^{-1}$, roughly the heating rate estimated for the bulk silicate Earth derived from a chondritic starting condition [Stacey, 1992]. Although the time series of the surface heat flux differs between the two models, the mean heat fluxes over the periods examined differ very little. With the specified heating mode, we find that the mean ratio of the basal to the surface heat flux in both models is roughly 0.4 [Gait *et al.*, 2008]. This value is at the low end, but within the range, of recent estimates of

the ratio of the mean core to mean mantle heat fluxes [Lay *et al.*, 2008]. A higher ratio could yield even more buoyant plumes which we suggest are likely to be even more robust than the plumes in our models.

[18] The mean nondimensional surface velocity of Model B is 1168. In the period modeled the average distance travelled by a particle on the surface is $4.2d$. Due to the significant increase in viscosity in the lower mantle of the model the magnitude of the mean horizontal velocity reduces significantly with depth. The highest horizontal velocities in the lower mantle occur at the bottom of the system and are slightly greater than 40% of the surface velocity. (Note this implies that the surface transit times quoted throughout this paper can be converted to lower mantle transit time by multiplying by 0.4.) If any of the plumes in the lower mantle had moved with such a velocity we should expect to see movement of the plume conduits of more than $1.5d$ during the periods modeled. Our findings don't indicate any such movement but show the lower mantle planform remains almost unchanged as plates move rapidly across the surface. Indeed, the bulk of the lower mantle in our calculations is characterized by horizontal velocities of approximately 10% of the mean plate velocities. It appears that a significant increase in lower mantle viscosity over upper mantle viscosity results in distinct time scales for upper and lower mantle convection so that plate geometries reconfigure at a pace that lower mantle velocities cannot respond to. Consequently, lower mantle thermal anomalies maintain relatively fixed positions for long periods in comparison with plate boundary evolution.

[19] We note that our models do not suggest that a factor of 90 increase in lower mantle viscosity relative to the upper mantle must preclude plume motion. Larger solution domains, featuring a greater number of plumes, and longer simulations may still reveal examples of isolated episodes of plume motion [Christensen, 1998; Tarduno, 2007] and should be examined in future work. However, our findings show that long periods characterized by plume immobility occur readily in an evolving 3D plate-mantle system featuring such a viscosity profile.

[20] **Acknowledgments.** JPL is grateful to the NSERC of Canada for continued funding in planetary mantle dynamics (327084-06).

References

- Christensen, U. (1998), Fixed hotspots gone with the wind, *Nature*, 391, 739–740.
- Davies, J. H. (2005), Steady plumes produced by downwellings in Earth-like vigor spherical whole mantle convection models, *Geochem. Geophys. Geosyst.*, 6, Q12001, doi:10.1029/2005GC001042.
- Gable, C. W., R. J. O'Connell, and B. J. Travis (1991), Convection in three dimensions with surface plates: Generation of toroidal flow, *J. Geophys. Res.*, 96, 8391–8405.
- Gait, A. D., J. P. Lowman, and C. W. Gable (2008), Time dependence in 3-D mantle convection models featuring evolving plates: Effect of lower mantle viscosity, *J. Geophys. Res.*, 113, B08409, doi:10.1029/2007JB005538.
- Jellinek, A. M., and M. Manga (2004), Links between long-lived hot spots, mantle plumes, D'' , and plate tectonics, *Rev. Geophys.*, 42, RG3002, doi:10.1029/2003RG000144.
- King, S. D., C. W. Gable, and S. A. Weinstein (1992), Models of convection-driven tectonic plates: A comparison of methods and results, *Geophys. J. Int.*, 109, 481–487.
- Koglin, D. E., Jr, S. R. Ghias, S. D. King, G. T. Jarvis, and J. P. Lowman (2005), Mantle convection with reversing mobile plates: A benchmark study, *Geochem. Geophys. Geosyst.*, 6, Q09003, doi:10.1029/2005GC000924.

- Lay, T., J. Hernlund, and B. A. Buffett (2008), Core-mantle boundary heat flow, *Nature Geosci.*, *1*, 25–32.
- Lowman, J. P., S. D. King, and C. W. Gable (2004), Steady plumes in viscously stratified, vigorously convecting, three-dimensional numerical mantle convection models with mobile plates, *Geochem. Geophys. Geosyst.*, *5*, Q01L01, doi:10.1029/2003GC000583.
- Lux, R. A., G. F. Davies, and J. H. Thomas (1979), Moving lithosphere plates and mantle convection, *Geophys. J.R. Astron. Soc.*, *57*, 209–228.
- Monnereau, M., and S. Quéré (2001), Spherical shell models of mantle convection with tectonic plates, *Earth Planet. Sci. Lett.*, *184*, 575–587.
- Quéré, S., and A. M. Forte (2006), Influence of past and present-day plate motions on spherical models of mantle convection: Implications for mantle plumes and hotspots, *Geophys. J. Int.*, *165*, 1041–1057.
- Stacey, F. D. (1992), *Physics of the Earth*, 3rd ed., Brookfield, Brisbane, Queensl., Australia.
- Steinberger, B., and R. J. O'Connell (1998), Advection of plumes in mantle flow: Implications for hotspot motion, mantle viscosity and plume distribution, *Geophys. J. Int.*, *132*, 412–434.
- Tackley, P. J. (1996), Effects of strongly variable viscosity on three-dimensional compressible convection in planetary mantles, *J. Geophys. Res.*, *101*, 3311–3332.
- Tarduno, J. A. (2007), On the motion of Hawaii and other mantle plumes, *Chem. Geol.*, *241*, 234–247.
- Zhong, S., M. T. Zuber, L. Moresi, and M. Gurnis (2000), Role of temperature-dependent viscosity and surface plates in spherical shell models of mantle convection, *J. Geophys. Res.*, *105*, 11,063–11,082.
-
- C. W. Gable, Hydrology, Geochemistry and Geology Group, Earth and Environmental Sciences Division, Los Alamos National Laboratory, Los Alamos, NM 87545, USA. (gable@lanl.gov)
- A. D. Gait, School of Mathematics, University of Manchester, Manchester M13 9PL, UK. (andrew.gait@manchester.ac.uk)
- H. Kukreja and J. P. Lowman, Department of Physical and Environmental Sciences, University of Toronto Scarborough, 1265 Military Trail, Toronto, ON M1C 1A4, Canada. (harish.kukreja@utoronto.ca; lowman@utsc.utoronto.ca)